Predicting the Speed of a Wave-Propelled Autonomous Surface Vehicle Using Metocean Forecasts

Henning Øveraas, Aksel Heggernes, Alberto Dallolio, Torleiv Håland Bryne, Tor Arne Johansen
Department of Engineering Cybernetics
Norwegian University of Science and Technology
Trondheim, Norway
Email: akselheg@stud.ntnu.no, {henning.overaas, alberto.dallolio, torleiv.h.bryne, tor.arne.johansen}
@ntnu.no

***Abstract*—Wave-propelled autonomous surface vehicles are becoming increasingly popular in oceanographic research due to their ability to provide persistent observations of the ocean environment. This type of vehicles are propelled purely by environmental forces which greatly enhances endurance. However, unlike vehicles with motorized propulsion, the velocity of wave-propelled autonomous surface vehicles cannot be controlled actively, making mission planning routines depend on predictions. In this work, we compare two methods based on linear regression and Gaussian process regression for predicting the speed of the wave-propelled autonomous surface vehicle AutoNaut. The regression models are trained using onboard measurements gathered during field operations, while the predictions are performed using metocean (wind, wave and current) forecasts. The Gaussian process regression model proves to be the most accurate way of predicting the speed of the vehicle.**

I. Introduction

Large scale climate changes make the ocean a continuously evolving environment. This represents a threat to biodiversity, and persistently monitoring the changes is a necessity. This motivates science-driven oceanic exploration, where observation of the upper water column by means of robotic systems has already been demonstrated [1], [2], [3], [4]. Today, ocean monitoring relies on robotic platforms or ship-based platforms as a supplement to remote sensing, e.g. [5]. Ship-based monitoring cannot scale over time or space and most robotic platforms are heavily constrained due to, for example, energy requirements and proximity to the shore or having the need of support vessels to operate.

This motivates the use of long-endurance robotic platforms with the capability of operating in harsh environments and for longer periods of time. An example of such platforms are green energy surface vehicles that harvest energy from the environment to sustain themselves for long missions. Several examples of these vehicles exist today, for example Liquid Robotics' Wave Glider [6], Offshore Sensing SailBuoy [7] and AutoNaut [8]. The common factor for all these platforms is that they rely on environmental forces such as wind and waves to propel themselves. This makes them durable and suitable of longer missions (e.g., weeks or months), but at the cost of losing the controllability of the speed. Without accurate prediction of the speed it will be impossible to accurately determine or plan where the vehicle will be in the future. Predicting the speed is therefore essential in scientific missions whose objectives require that the autonomous surface vehicle (ASV) is at the right place at the right time, e.g., missions designed to map or track phytoplankton blooms at a given place at a given time.

Various methods for predicting the speed of wave-propelled vehicles have already been tested. In [9], [10], [11] the speed is predicted with both linear and Gaussian process regression for the Wave Glider. In this work we apply the speed prediction techniques used in [9], [10], [11] on the AutoNaut, a commercially available ASV whose propulsion is mainly generated from surface waves [8]. We employ a version of the ASV in which the control system is designed and built by the Norwegian University of Science and Technology (NTNU), as described in [12]. Unlike the Wave Glider, the AutoNaut is equipped with submerged hydrofoils that are rigidly connected to the hull to convert wave-induced pitching motion into forward velocity.

II. Method

To predict the speed we aim to find a function f such that $y = f(\boldsymbol{x})$, where $y \in \mathbb{R}$ is the speed of the vehicle and $\boldsymbol{x} \in \mathbb{R}^n$ is a n-dimensional feature vector containing relevant environmental variables. We try two different prediction methods, linear regression and Gaussian process regression.

A. Linear Regression

The linear regression model can be expressed as

$$y = f(\boldsymbol{x}) = \boldsymbol{w}^\intercal \boldsymbol{x} \tag{1}$$

where $\boldsymbol{w}$ is a vector containing a set of weights and $\boldsymbol{x}$ is a set of known features. The vector $\boldsymbol{w}$ is found by minimising the squared error between the matrix of training features $\boldsymbol{X}$ and the corresponding matrix of output variables $\boldsymbol{Y}$:

$$\boldsymbol{w} = (\boldsymbol{X}^\intercal \boldsymbol{X})^{-1} \boldsymbol{X}^\intercal \boldsymbol{Y} \tag{2}$$

B. Gaussian Process Regression

Gaussian process regression (GPR) is a non-parametric, Bayesian prediction method. Instead of calculating the probability distribution for parameters from a specific function, the GPR considers all smooth functions within a certain domain that can fit the data. Then, the GPR computes the joint probability distribution over functions that fit the data for a set of points. It has the general form

$$y = f(\boldsymbol{x}) \sim GP(m(\boldsymbol{x}), k(\boldsymbol{x}, \boldsymbol{x}')) \tag{3}$$

where $m(\boldsymbol{x})$ and $k(\boldsymbol{x}, \boldsymbol{x}')$ are the mean and covariance functions [13]. Similarly to [9], [10], [11], we let the mean function be zero and use a Matérn-class covariance function, expressed as

$$k_{mat}(\boldsymbol{x}, \boldsymbol{x}') = \frac{2^{1-v}}{\Gamma(v)} \left(\frac{\sqrt{2v}(\boldsymbol{x} - \boldsymbol{x}')}{l} \right)^{2} K_v \left(\frac{\sqrt{2v}(\boldsymbol{x} - \boldsymbol{x}')}{l} \right), \tag{4}$$

where v and l are positive parameters, and K_v is a modified Bessel function [14].

C. Bootstrap Aggregation

Bootstrap aggregation is an ensemble learning method used to combat over-fitting. The process involves generating T different training set from the original training data by using bootstrap sampling, that is random sampling with replacement. The base learner is then trained by applying the learning algorithm on each subset independently. The T outputs are then aggregated to get the final results. For regression problems the most common aggregation method is to take the average. For further reading see [15].

D. Forecast

The forecast model used in this work is the Norwegian NordKyst800m forecast model [16] based on the Regional Ocean Modeling System [17]. The forecast model has a spatial resolution of 800×800 meters and a temporal resolution of 1 hour. The relevant information provided by the forecast model is wind direction, wind speed, significant wave height, peak wave frequency, current direction and current speed.

The vehicle is equipped with a differential GNSS (dGNSS) receiver[1] which provides measurements of the position, speed over ground and heading. The heading is derived from the differential position measurement using the moving base RTK technique. The vehicle is also equipped with a weather station[2], hence measurements of the wind speed and direction can be obtained directly. In addition, estimates of the wave height and wave frequency can be obtained by processing the height measurement, h, provided by the dGNSS receiver [18]. According to [19], we assume that the wave height follows a Rayleigh distribution and that the significant wave height can be estimated as

$$H_s = 1.416 H_{rms}\mathrm{m}, \tag{5}$$

[1]https://www.hemispheregnss.com/product/vector-v200-gnss-smart-antenna/

[2]https://www.airmar.com/weather-description.html?id=152

where H_{rms} is the root-mean-square wave height given by

$$H_{rms} = \sqrt{\frac{1}{N} \sum_{i=1}^{N} h_i^2}. \tag{6}$$

By splitting the data into batches of N measurements the significant wave height can be computed for each batch. The wave encounter frequency ω_e can be estimated by measuring the time difference between the peaks in the height measurements. The peak wave frequency can then be estimated by solving the equation

$$\omega_e = \left| \omega_p - \frac{\omega_0}{g} U \cos \gamma_{wave} \right| \tag{7}$$

where ω_p is the peak frequency, g is the gravitational acceleration, U is the speed over ground of the vehicle and γ_{wave} is the wave angle of attack [20].

By comparing the forecast with its corresponding estimate from the measured values onboard the vehicle we can validate the accuracy of some of the forecast. Figure 1 and 2 show the forecast and measurement of the relative wind and significant wave height for 3312 data samples of 5 minutes each, totaling a period of approximately 200 hours. Measurements are collected at Frohavet on the north-west coast of Norway in a period from April 2020 to April 2021. The forecast is downloaded from the Nordkyst800m model for the corresponding times and locations. Figures 1 and 2 show a strong correlation between the measurement and forecast, thus we expect that the forecast is reasonably accurate. The forecast and estimate of the significant wave height show a difference in magnitude. The estimate of the significant wave height is computed using the raw heave measurement from the dGNSS receiver, which can have a poor accuracy, due to, for example, satellite geometry [21].

Further, Figure 3 shows how the relevant environmental features from the forecast correlate to the measured speed over ground of the vehicle.

E. Environmental Features

For a wave-propelled ASV the speed is a result of the forces caused by the environment. We therefore use the properties of wind, waves and currents as features in the speed prediction models. The speed over ground (U) is available from the dGNSS receiver onboard the vehicle. The wave height, wave frequency, wave direction, current speed, current direction, wind speed and wind direction are all obtained from the forecasts. The forecasts of the wind, current and waves are provided in a two-dimensional local coordinate frame with x-axis pointing towards north and y-axis pointing towards east. The effect of the environmental forces on the vehicle will depend on their direction relative to the vehicle's heading and therefore it is necessary to introduce a body-fixed reference frame. We denote the forecast's reference frame as $\{n\}$. Further, we define a body-fixed reference frame, denoted $\{b\}$, with its origin in the centre of mass of the vehicle, the x-axis pointing towards the front, the z-axis pointing down and the y-axis completing the right hand coordinate system. We

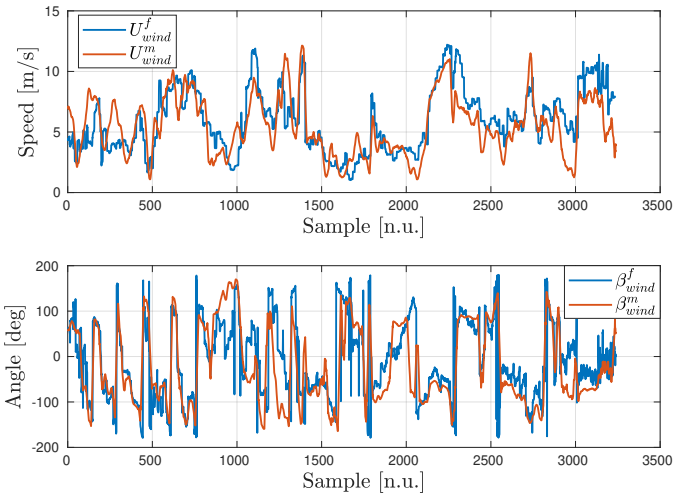

Fig. 1. A comparison of the wind speed from the forecast (U^f_{wind}) and measurement (U^m_{wind}) (top) and a comparison of wind direction relative to north from the forecast (β^f_{wind}) and measurement (β^m_{wind}) (bottom).

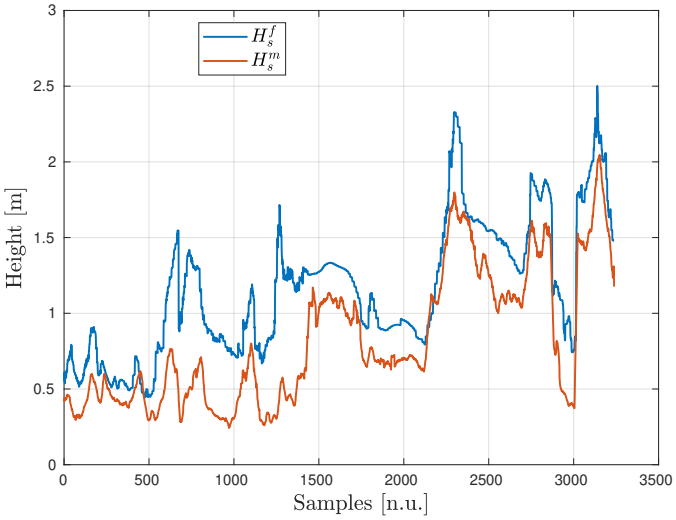

Fig. 2. A comparison of significant wave height from the forecast (H^f_s) and significant wave height estimated from measurements (H^m_s).

only consider horizontal motion of the vehicle, then a vector $\boldsymbol{x}^n = \begin{bmatrix} x^n & y^n \end{bmatrix}^\mathsf{T}$ in the forecast frame can be converted to the body frame with the rotation

$$\begin{bmatrix} x^b \\ y^b \end{bmatrix} = \begin{bmatrix} \cos\psi & \sin\psi \\ -\sin\psi & \cos\psi \end{bmatrix} \begin{bmatrix} x^n \\ y^n \end{bmatrix}, \tag{8}$$

where ψ is the heading of the vehicle measured by the dGNSS receiver. For a velocity vector $\boldsymbol{x}^b = \begin{bmatrix} u & v \end{bmatrix}^\mathsf{T}$ in the body frame, the angle of attack γ and magnitude U of an environmental force are computed as

$$\gamma = \arctan\left(\frac{v}{u}\right) \tag{9}$$

and

$$U = \sqrt{u^2 + v^2}. \tag{10}$$

We expect the linear regression model to handle nonlinearities

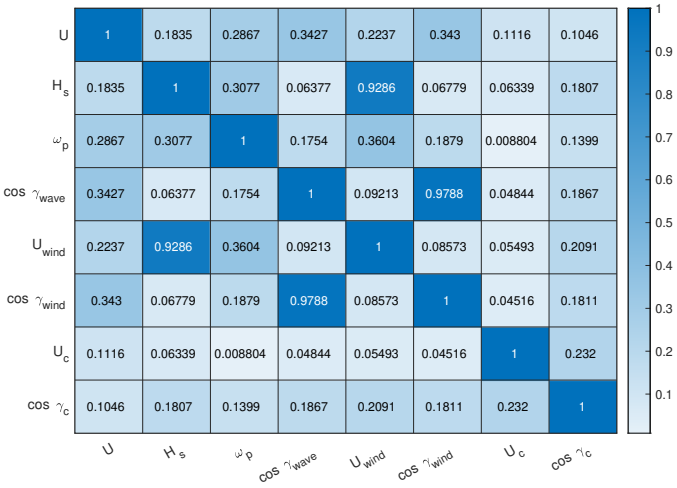

Fig. 3. Correlation matrix showing the absolute value of the correlation coefficient for the environmental features used in the feature vector for the GPR models and the speed over ground for the vehicle (U).

poorly. Hence, we transform the wind and currents to $\{b\}$ and use only the velocity component in the x-direction as features. The feature vector for the linear model is then given by

$$\boldsymbol{x} = \begin{bmatrix} H_s & \omega_p & \cos\gamma_{wave} & u_{wind} & u_c & 1 \end{bmatrix}^\mathsf{T}, \tag{11}$$

where H_s is the significant wave height, ω_p is the peak wave frequency, γ_{wave} is the wave angle of attack, u_{wind} is the wind velocity along the x-axis in $\{b\}$ and u_c is the current velocity along the x-axis in $\{b\}$. The final term in the feature vector is a bias term. By taking the cosine of the wave angle we normalize the angle such that $\gamma_{wave} \in [-1, 1]$.

It is expected that the GPR model is able to handle nonlinearities in the data better than the linear model. We therefore alter the feature vector to

$$\boldsymbol{x} = \begin{bmatrix} H_s & \omega_p & \cos\gamma_{wave} & U_{wind} & \cos\gamma_{wind} & U_c & \cos\gamma_c \end{bmatrix}^\mathsf{T}, \tag{12}$$

where U_{wind} is the wind speed, γ_{wind} is the wind angle of attack, U_c is the current speed and γ_c is the current angle of attack. By including the angle of attack and speed as features directly instead of including them as body-fixed velocities we include any effects the forces in the lateral direction on the vehicle may have on the total speed as well.

The environmental forces (generated from wind, currents and waves), usually show of a low frequency component and a high frequency component. For the wind, the low frequency component is due to the slowly varying wind speed, while the high frequency component is due to gusts. We can assume the speed of the vehicle is also going to be a sum of a low frequency component and a high frequency component. Predicting the high frequency variations in speed is of little interest and we therefore remove it by averaging the data over a period of 5 minutes.

III. Results

Both prediction methods are trained using forecast data and the measured speed over ground from the vehicle. The data

is collected during several field campaigns spanning a 1 year period. The data is split into a training set (80%), validation set (10%) and testing set (10%), where the validation set is used when tuning and selecting the appropriate features to prevent over-fitting the models to the test set. For the GPR model a Matérn-class covariance function with $v = 3/2$ is used. The trained models is then used to predict the speed based on forecast data. For the training data the heading is known and the correct angle of attack for wind, current and waves can be computed directly. In the dataset used for testing, the heading is considered unknown and the constant heading toward the next waypoint is used instead.

Figures 4 and 5 show the predictions using linear regression, Gaussian process regression and Gaussian process regression with bootstrap aggregation for the testing set. The data is collected over 3 days with varying conditions. Case 1 shows a time series of approximately 20 hours of data and case 2 consists of approximately 13 hours. In both cases all three prediction models manage to predict the major changes in speed over ground for the vehicle. Figure 6 and 7 show the cumulative velocity error (i.e., distance error) for all three prediction models in both cases. We define the cumulative velocity error as

$$CVE := \sum_{i=1}^{N} \left(U_i - \hat{U}_i \right), \tag{13}$$

where U is the measured speed over ground and $\hat{U}$ is the predicted speed over ground. The models using GPR give the smallest distance error and are thus the models that give the most consistent prediction for both cases. In practice, this means that when predicting the vehicle's position in the future using the predicted speed we will end up closest to the desired point using the GPR model with bootstrap aggregation for case 2 and the GPR model without bootstrap aggregation for case 1. In both cases the linear model will give the largest distance error at the end of the simulation.

We are also interested in how the magnitude of the CVE develops as the total distance traveled increases. We therefore define the normalized cumulative velocity error as

$$NCVE := 100\% \times \sum_{i=1}^{N} \left(\frac{U_i - \hat{U}_i}{d_i} \right), \tag{14}$$

where d_i is the distance traveled between two data samples. Figure 8 and 9 show the $NCVE$ for all three models in case 1 and case 2, respectively. Here we can see that the cumulative velocity error for the GPR model with bootstrap aggregation will get close to zero percent of the total traveled distance in both cases. The two other models, on the other hand, will not. This indicates the presence of a bias in the two simplest models.

IV. Discussion

We cannot expect all forecasts to be completely accurate at all times. As mentioned, the spatial and temporal resolutions of the forecast are 800×800 meters and 1 hour respectively,

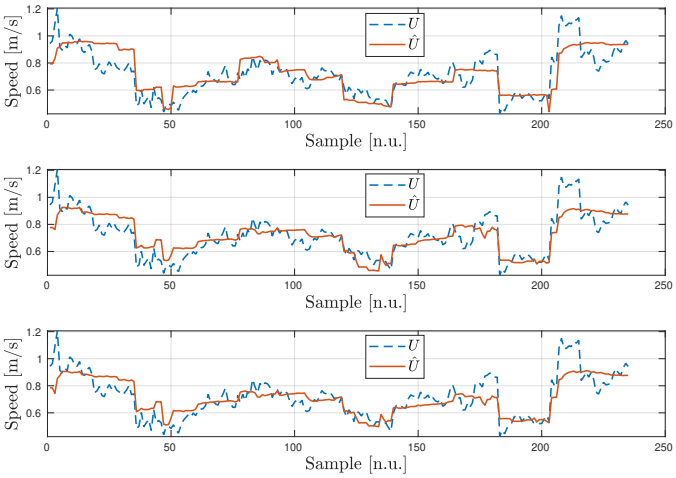

Fig. 4. Case 1: Predicted ($\hat{U}$) compared to true (U) speed over ground for a period of approximately 20 hours using the liner model (top), Gaussian process model (middle) and Gaussian process model with bootstrap aggregation (bottom).

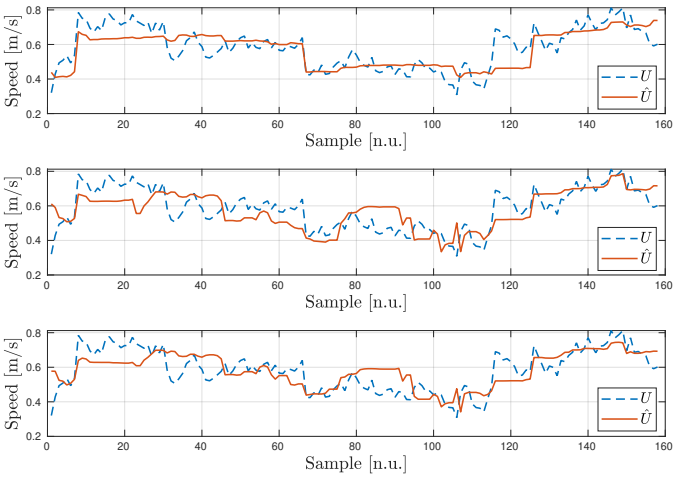

Fig. 5. Case 2: Predicted ($\hat{U}$) compared to true (U) speed over ground for a period of approximately 13 hours using the liner model (top), Gaussian process model (middle) and Gaussian process model with bootstrap aggregation (bottom).

thus any local variation in the ocean environment within these boundaries are not captured. This can be observed in both Figures 4 and 5, where all prediction models fail to account for small local variations of the environmental conditions resulting in an erroneous speed over ground prediction. In particular, we expect the ocean current to show unpredictable local variations due to, for example, variation in ocean depth, the vehicles proximity to river outlets or small islands. Previous works have shown that the ocean current has a large effect on the speed for this type of vehicle [22], and errors in the forecast may explain some of the inconsistencies in the predictions.

Even though the forward propulsion force of the vehicle is primarily a function of the wave-induced motion, the correlation matrix in Figure 3 shows that the current and particularly the wind have a significant effect on the total

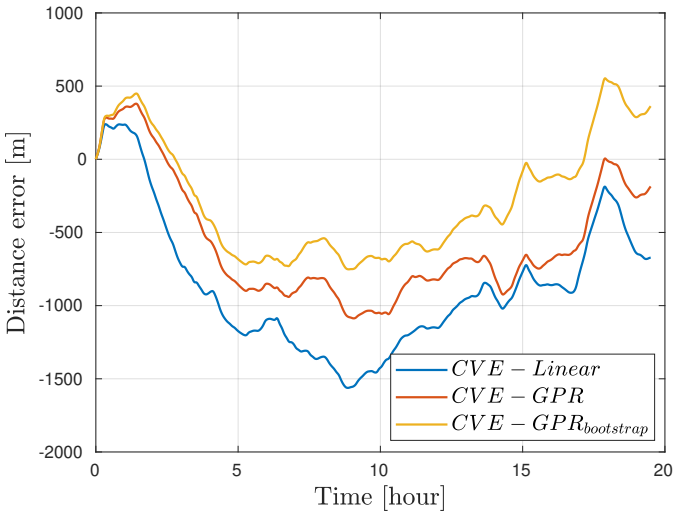

Fig. 6. Case 1: Cumulative error for the speed prediction over approximately 20 hours for all models.

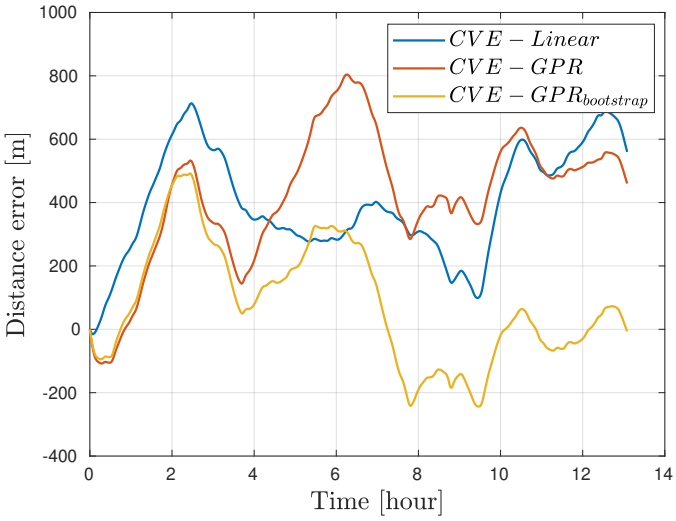

Fig. 7. Case 2: Cumulative error for the speed prediction over approximately 13 hours for all models.

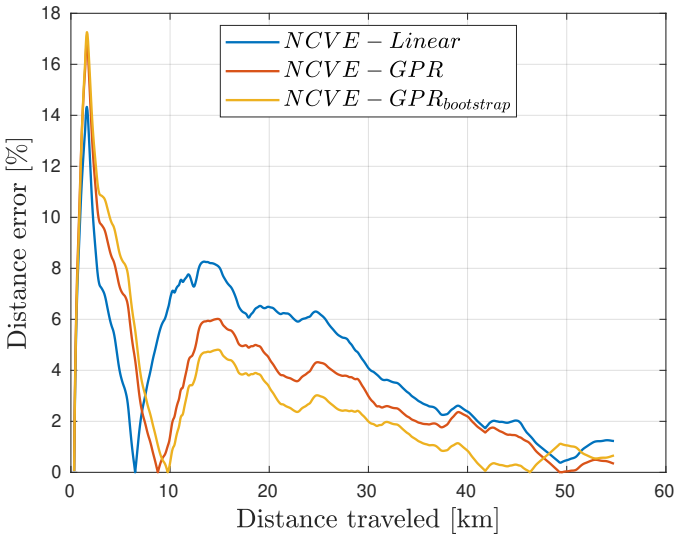

Fig. 8. Case 1: Normalized cumulative error for the speed prediction over approximately 20 hours for all models.

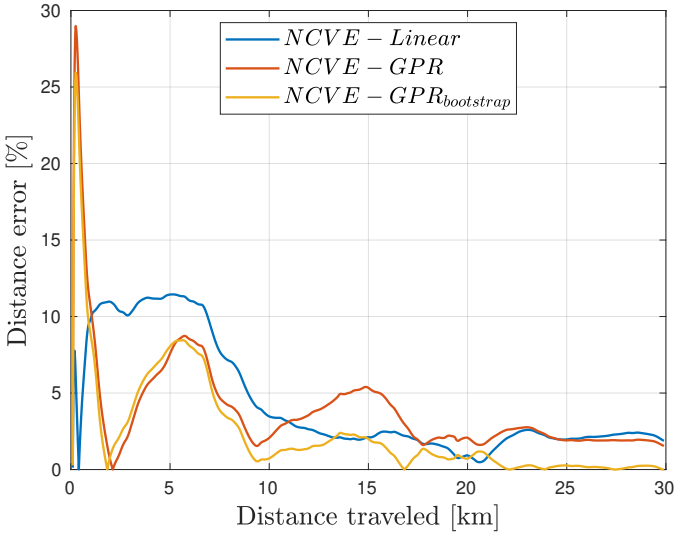

Fig. 9. Case 2: Normalized cumulative error for the speed prediction over approximately 13 hours for all models.

speed of the vehicle. The absolute value of the correlation coefficient between the cosine of the wind direction and the speed over ground is $R = 0.343$, thus having a favorable angle of attack to the wind is equally important as the significant wave height and wave period to achieve a high total speed. The importance of the wind and current on the speed over ground of the vehicle further complicate the prediction of the local variations in speed, as particularly the current commonly have a larger spatial variation compared to the wave height and wave frequency [19].

Both cases shown in Figures 4 and 5 show poor accuracy in the prediction whenever the speed is high, particularly in case 1 where the speed is above $1.5\,\mathrm{m/s}$ at times. The AutoNaut has a nominal speed of $0.5\,\mathrm{m/s}$ to $1.5\,\mathrm{m/s}$, but rarely reaches speeds above $1\,\mathrm{m/s}$. Figure 10 shows the distribution of the training data with respect to the speed. The majority of the data shows that the vehicle moves at a speed between $0.2\,\mathrm{m/s}$ to $0.8\,\mathrm{m/s}$ and only small amounts of data are collected where the speed is above $1.5\,\mathrm{m/s}$. For this reason, the poor predictions at higher speeds in the test data can be explained by a lack of representative training data. We also consider the possibility that the speed of the vehicle is affected by additional properties of the environmental forces not considered here, for example the directional spread of the waves.

V. Conclusion

In this work, two different regression models have been used to predict the speed of the AutoNaut. The models were trained using a combination of forecast data and measurements collected during field experiments conducted by the AutoNaut

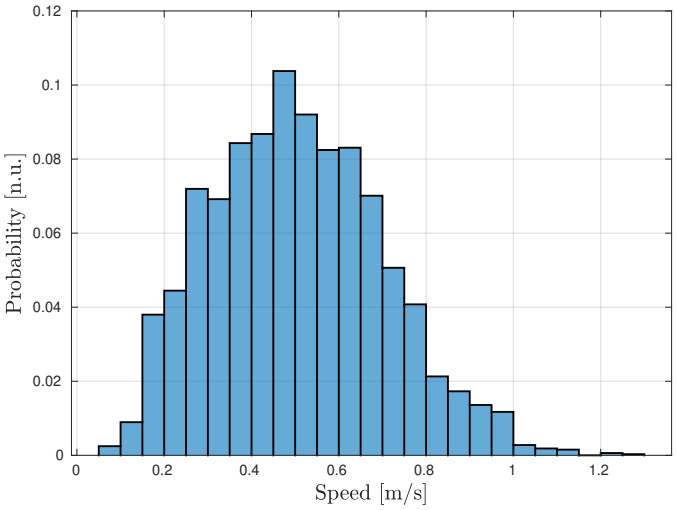

Fig. 10. Distribution of the speed over ground measurements in the training data.

ASV. A speed prediction was then obtained by predicting on forecast data. Both models were successful in capturing the the majority of dynamical behaviour of the speed. However, the spatial and temporal scale of the forecast limits the accuracy of the prediction on shorter horizons. The Gaussian process model provides a more consistent prediction and is shown to be the favorable model when the predicted speed is used to determine an end-position for a vehicle navigation over a known time interval.

ACKNOWLEDGMENT

This work was supported by the Research Council of Norway (RCN) through the MASSIVE project, grant number 270959, and the center of excellence (AMOS) grant number 223254. The authors would like to thank Pedro De La Torre for the support with the operations and logistics.

REFERENCES

[1] A. S. Ferreira, M. Costa, F. Py, J. Pinto, M. A. Silva, A. Nimmo-Smith, T. A. Johansen, J. B. de Sousa, and K. Rajan, "Advancing multi-vehicle deployments in oceanographic field experiments," *Autonomous Robots*, Oct 2018. [Online]. Available: https://doi.org/10.1007/s10514-018-9810-x

[2] M. J. Costa and et.al, "Field report: Exploring fronts with multiple robots," in *IEEE AUV*, Porto, 2018.

[3] P. McGillivary, J. Borges de Sousa, R. Martins, K. Rajan, and F. Leroy, "Integrating autonomous underwater vessels, surface vessels and aircraft as persistent surveillance components of ocean observing studies," in *2012 IEEE/OES Autonomous Underwater Vehicles (AUV)*, Sep. 2012, pp. 1–5.

[4] J. N. Cross, C. W. Mordy, H. M. Tabisola, C. Meinig, E. D. Cokelet, and P. J. Stabeno, "Innovative technology development for arctic exploration," in *OCEANS 2015 - MTS/IEEE Washington*, 2015, pp. 1–8.

[5] A. Dallolio, G. Quintana-Diaz, E. Honoré-Livermore, J. Garrett, R. Birkeland, T. A. Johansen, "A satellite-USV system for persistent observation of mesoscale oceanographic phenomena," *Remote Sensing*, 2021.

[6] R. Hine, S. Willcox, G. Hine, and T. Richardson, "The wave glider: A wave-powered autonomous marine vehicle," in *OCEANS 2009*, Oct 2009, pp. 1–6.

[7] I. Fer and D. Peddie, "Near surface oceanographic measurements using the sailbuoy," in *2013 MTS/IEEE OCEANS - Bergen*, June 2013, pp. 1–15.

[8] P. Johnston and M. Poole, "Marine surveillance capabilities of the autonaut wave-propelled unmanned surface vessel (usv)," in *OCEANS 2017 - Aberdeen*, June 2017, pp. 1–46.

[9] P. Ngo, W. Al-Sabban, J. Thomas, W. Anderson, J. Das, R.N Smith, "An analysis of regression models for predicting the speed of a wave glider autonomous surface vehicle," *Proceedings of Australasian Conference on Robotics and Automation*, Dec. 2013.

[10] R.N. Smith, J. Das, G. Hine, W. Anderson, and G.S. Sukhatme, "Predicting wave glider speed from environmental measurements," *Proceedings of the MTS/IEEE Oceans '11 - Kona*, Sep. 2011.

[11] P. Ngo, J. Das, J. Ogle, J. Thomas, W. Anderson, and R.N. Smith, "Predicting the speed of a wave glider autonomous surface vehicle from wave model data," *2014 IEEE/RSJ International Conference on Intelligent Robots and Systems*, sep, 2014.

[12] A. Dallolio, B. Agdal, A. Zolich, J.A. Alfredsen, and T.A. Johansen, "Long-endurance green energy autonomous surface vehicle control architecture," *IEEE/MTS OCEANS*, Seatle, 2019.

[13] C. E. Rasmussen and C.K.I. Williams, *Gaussian processes for machine learning*. MIT Press, 2006.

[14] M. Abramowitz and I.A Stegun, *Handbook of Mathematical Functions with Formulas, Graphs, and Mathematical Tables*. Dover Publications Inc., New York, pp.1046, 1965.

[15] Z.-H. Zhou, "Ensemble methods: Foundations and algorithms," 2012.

[16] Norwegian Meteorological Institute. (2018) Norkyst 800 v2. [Online]. Available: https://thredds.met.no/thredds/fou-hi/norkyst800v2.html

[17] A. Shchepetkin and J. McWilliams, "The regional oceanic modeling system (roms): a split-explicit, free-surface, topography-following- coordinate ocean model," *Ocean Modelling*, vol. 9, pp. 347–404, 12 2005.

[18] A. Dallolio, J. A. Alfredsen, T. I. Fossen, and T. A. Johansen, "Experimental validation of a nonlinear wave encounter frequency estimator onboard a wave-propelled usv," in *IFAC Conference on Control Applications in Marine Systems, Robotics, and Vehicles*, 2021.

[19] R.G Dean and R.A Dalrymple, *Water Wave Mechanics for Engineers and Scientists*. World Scientific, pp. 193, 1991.

[20] T. Fossen, *Handbook of Marine Craft Hydrodynamics and Motion Control*. John Wiley & Sons, 2021.

[21] P. Groves, *Principles of GNSS, Inertial, and Multisensor Integrated Navigation Systems, Second Edition*, 03 2013.

[22] A. Dallolio, H. Øveraas, and T. A. Johansen, "Gain-Scheduled Steering Control for a Wave-Propelled Unmanned Surface Vehicle," 2021, Ocean Engineering (submitted).